RSC Advances

ROYAL SOCIETY OF CHEMISTRY

www.rsc.org/advances

Cite this: DOI: 10.1039/c0xx00000x

www.rsc.org/xxxxxx ARTICLE TYPE

Modification of the emission colour and quantum efficiency for oxazoline- and thiazoline-containing iridium complexes via different N^O ligands

Yanling Si[a], Shuai Zhang[a], Godefroid Gahungu[d], Jinghai Yang*[b] and Zhijian Wu*[c]

Received (in XXX, XXX) Xth XXXXXXXXX 20XX, Accepted Xth XXXXXXXXX 20XX
DOI: 10.1039/b000000x

DFT/TDDFT method was applied to explore the geometrical, electronic and photophysical properties of recently reported oxazoline- and thiazoline-containing iridium(III) complexes [(ppy)$_2$Ir(oz)] (**1**) and [(ppy)$_2$Ir(thoz)] (**2**). The calculated absorption and emission wavelengths are in agreement with experimental data. Based on complexes **1** and **2**, a series of Ir(III) complexes **3**, **4**, **5** and **6** with different N^O ligands have been designed. The calculated results reveal that the different ancillary ligands not only affect the absorption spectra properties but also tune the emission colour. Compared with **2**, the higher quantum yield of experimental observation for **1** was explained by its larger MLCT contribution and smaller singlet-triplet splitting energy (ΔE_{S1-T1}). From this point of view, the designed complexes **3**, **5** and **6** are expected to be potential phosphorescence emitters in OLEDs with high quantum efficiency.

1. Introduction

Transition metal Iridium complexes with phosphorescent properties have increasingly attracted a lot of attention, especially in the application of organic light-emitting diodes (OLEDs).[1-4] Transition metal atoms own strong spin–orbit coupling effects, which can enhance the intersystem crossing from the singlet to the triplet excited state, leading to a high phosphorescence efficiency.[5,6] Thus, numerous attempts have been made to explore the transition metal complexes as phosphorescent emitters. Moreover, Ir(III) complexes also have high thermal stability, high photo luminescence efficiency, short excited-state lifetime, and good emission wavelength tunability.[7-10]

For realizing the full-color displays, many interesting Ir(III) complexes emitting green (such as Ir(ppy)$_3$ and Ir(dfppy)$_2$(acac), ppy = 2-phenylpyridine, dfppy = 4,6-difluoro-phenylpyridine, acac = acetylacetonate), red (such as Ir(piq)$_3$, piq = 1-phenylisoquinolato), blue (such as Ir(dfppy)$_2$(pic), pic = picolate), and other colors have been developed with good device performances.[11-18] Recently, Chao et al. reported two new oxazoline- and thiazoline-containing Ir(III) complexes [(ppy)$_2$Ir(oz)] (**1**) and [(ppy)$_2$Ir(thoz)] (**2**)[19] (ppy =2-phenylpyridine), oz=(2-(2'-hydroxyphenyl)-2-oxazoline) and thoz= (2-(2'-hydroxyphenyl)-2-thiazoline) with high efficient electroluminescence (EL) performance and emission colors of green and yellow. They also performed a time-dependent density functional theory (TDDFT) study on the absorption spectra of the synthesized complexes. The reliability of TDDFT method was demonstrated from the good agreement between the calculated and experimental absorption spectra.[19] Encouraged by the work by Chao et al., we designed a series of Ir(III) complexes **3**, **4**, **5** and **6** (Fig.1) on the basis of the experimental structures **1** and **2**. Compared with red and green emitters, blue-emitting materials with high efficiency and good stability remain a great challenge. Previous studies suggested that the substitution with electron-withdrawing nitrogen (N) atom plays an important role in realizing blue-emitting properties.[20,21] Assuming that this strategy can also hold for the complexes **1** and **2**, some blue emitting analogues can be expected. Exploring how the strategy can affect the photophysical properties of the complexes was the main objective of this work. In particular, the influence of the different N^O ligands on the quantum efficiency was investigated, which will be of great benefit for designing novel, high efficient blue-emitting Ir(III) complexes.

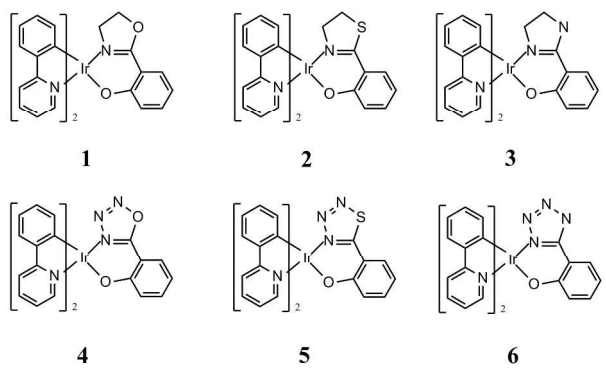

Fig. 1 Schematic structures of the complexes **1**-**6**.

2. Computational methodology

The ground state and the lowest-lying triplet excited state geometries for each complex were optimized by using the density functional theory (DFT)[22] with the hybrid-type Perdew-Burke-Ernzerhof exchange correlation functional (PBE0) and the unrestricted PBE0 (UPBE0), respectively,[23-25] which have been proved to be efficient and accurate for the calculation of transition metal complexes.[26] Herein, the ground state geometries of open-shell singlet with UPBE0 functional for complexes 1 and 2 were also optimized. The results show that the singlet calculations with UPBE0 functional give the same energies and geometries as the close-shell PBE0 calculations, confirming that PBE0 functional is enough to describe the ground state singlet. To confirm that each configuration was a minimum on the potential energy surface, vibrational frequencies were calculated at the same theoretical level.

On the basis of ground geometry optimization, TDDFT[27]/PBE0 calculations associated with the polarized continuum model (PCM)[28] in dichloromethane (CH_2Cl_2) media were applied to investigate the absorption properties. With respect to the emission properties, we performed a series of computations on the complexes 1 and 2 with five different functionals (PBE0, M062X[29], M052X[30], B3LYP[31] and Cam- B3LYP[32]). Our results indicated that M052X is more accurate in reproducing the experimental data (Table S1, Supporting Information). Therefore, M052X was selected in the calculation of emission spectra.

The"double-ξ"quality basis set LANL2DZ associated with the pseudopotential was employed on atom Ir and the 6-31G(d)[33] basis set was used for non-metal atoms in the gradient optimizations. All calculations were performed with the Gaussian 09 software package[34]. The Molekel 4.3.2 user interface[35] was used to manipulate the structures and orbitals.

3. Result and discussion

3.1 Molecular Geometries in Ground and Excited States

In the present work, we mainly focus on the structures of the singlet ground state (S_0) and the lowest triplet excited state (T_1) since they are involved in the phosphorescence process. The schematic structures of the studied complexes are presented in Fig. 1, and the optimized geometrical structures for complexes **1** and **2** in the ground states are shown in Fig. 2, along with the numbering of some key atoms. PBE0, B3LYP and M052X optimized bond lengths for **1** in S_0 state together with the X-ray crystal diffraction data[19] are listed in Table 1. The corresponding data for **2** are listed in Table S2 of Supporting Information. The percentage error (δ) indicates that the PBE0 functional provides a better accuracy (small δ) than M052X functional and the widely used hybrid B3LYP in the prediction of bond lengths.

Table 2 gives the Ir-related bond lengths for complexes **1-6** using the PBE0/LANL2DZ-6-31G(d) method. From Table 2, one can find that the Ir-N1 and Ir-N2 bond lengths of complex **3** are slightly decreased compared with those of **1** and **2**. Table 2 also shows that Ir–N1 and Ir–O1 bond lengths of complexes **4**, **5** and **6**, where C-C bond is replaced with N-N bond, are longer than those for **1**, **2** and **3**. This change is more obvious for **6**, due to the enhanced inter-molecular π-conjugation of tetrazole ring in ancillary ligand.

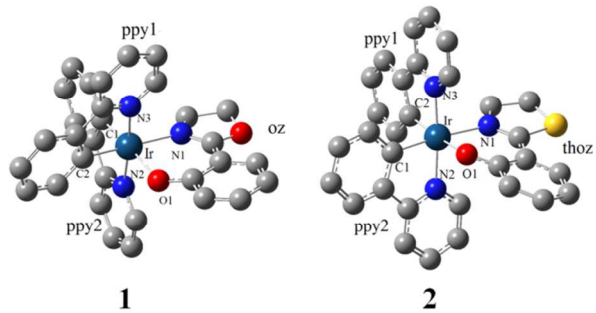

Fig. 2 Optimized ground state structures of complexes **1** and **2**.

The geometrical parameters of the studied complexes in the lowest triplet excited states are also listed in Table 2 to show the geometry changes upon excitation. Compared with S_0 states, most of the bond distances of **1-6** are shortened in T_1 states. Especially, the Ir-O1 bond length of **6** is obviously decreased in T_1 states. These changes indicate that the interaction between the metal and ancillary ligands will be strengthened in T_1 states.

Table 1 Selected optimized parameters for complex **1** in the ground statefrom different density functionals

		PBE0		B3LYP		M052x	
	Exp.[a]	Calc.[b]	δ[c]	Calc.[b]	δ[c]	Calc.[b]	δ[c]
Ir-N1	2.124	2.155	1.46	2.196	3.39	2.175	2.40
Ir-N2	2.035	2.036	0.05	2.060	1.23	2.050	0.74
Ir-N3	2.046	2.047	0.05	2.072	1.27	2.065	0.93
Ir-O1	2.146	2.156	0.47	2.182	1.68	2.172	1.21
Ir-C1	1.988	1.993	0.25	2.014	1.31	1.989	0.05
Ir-C2	2.006	2.002	-0.20	2.019	0.65	1.997	-0.45

[a] Crystal data from (ref. 19). [b]Calculated. [c] $\delta(\%)=\frac{calc-\exp}{\exp}\times 100$

Table 2 Main optimized bond distances (Å) of the complexes **1-6** in the singlet ground and the lowest lying triplet states

	1		**2**		**3**	
	S_0	T_1	S_0	T_1	S_0	T_1
Ir-N1	2.155	2.166	2.169	2.098	2.148	2.153
Ir-N2	2.036	2.018	2.050	2.062	2.033	2.018
Ir-N3	2.047	2.071	2.036	2.029	2.046	2.074
Ir-O1	2.156	2.143	2.144	2.125	2.162	2.147
Ir-C1	1.993	1.966	2.001	2.022	1.993	1.967
Ir-C2	2.002	1.997	1.995	1.996	2.004	1.999
	4		**5**		**6**	
	S_0	T_1	S_0	T_1	S_0	T_1
Ir-N1	2.161	2.140	2.175	2.134	2.159	2.142
Ir-N2	2.039	2.041	2.049	2.056	2.036	2.039
Ir-N3	2.050	2.051	2.038	2.035	2.049	2.060
Ir-O1	2.179	2.163	2.168	2.132	2.182	2.111
Ir-C1	1.993	1.991	1.996	2.010	1.992	1.987
Ir-C2	1.995	2.005	1.994	1.992	1.996	1.996

Furthermore, the difference in both ground and excited states will make a great effect on the frontier molecular orbitals, resulting in different electron transition characters.

3.2 Frontier molecular orbital (FMO) analysis

The character of the FMO and the HOMO (highest occupied molecular orbital)-LUMO (lowest unoccupied molecular orbital) energy gap are known to have influence on the properties of the complexes. Therefore, we will discuss the ground state electronic structure with special emphasis on the HOMO and LUMO. The contour plots of HOMO and LUMO of complexes **1**, **3**, **4** and **6** are presented in Fig. 3, while those for complexes **2** and **5** can be found in Fig. S1.

The HOMO of complex **1** is mainly localized on the d(Ir) and π(oz), while the composition of LUMO is predominantly contributed by the π*(ppy).[19] Compared with complex **1**, the HOMO and LUMO of complex **4** have markedly different distribution. The HOMO of the complex **4** is mainly contributed by d(Ir) and π(ppy), while the LUMO is exclusively localized on the N^O ligand, implying that the composition of FMOs is drastically influenced by different N^O ligands The same changes also occur from **2** to **5** (Fig. S1). For complexes **3** and **6**, the LUMOs are mainly localized on the ppy ligands, but with the different site (ppy1 for **3** and ppy2 for **5**). In comparison with being localized on the N^O ligand and the Ir d orbitals in the complex **3**, a significant difference is, however, observed for the HOMO of complex **6**, which is attributed to the ppy ligands with a mixture of Ir(d) character.

On the other hand, the different N^O ancillary ligands also affect the FMO energy levels. The calculated HOMO-LUMO energy gaps of complexes of **3**, **4**, **5** and **6** are 3.35 eV, 3.39 eV, 3.00 eV and 3.54 eV, respectively. Compared with the previous theoretical energy gaps for **1** and **2** (3.22 eV for **1** and 2.83 eV for **2**)[19], complexes **4** and **6** have larger HOMO-LUMO energy gaps. It is worth noting that complex **6** has the largest HOMO-LUMO energy gap among the studied complexes, which will affect the absorption and emission wavelengths.

3.3 Absorption spectra

TDDFT calculations are widely used to calculate the absorption properties of Ir(III) complexes on the basis of the optimized geometries.[36] Here, five different functionals (PBE0, M062X, M052X, B3LYP and Cam-B3LYP) were used to assess the effect of different DFT functionals on the absorption spectra of the complexes **1** and **2** (Table S3). It was found that the absorption wavelengths (nm) of the complexes **1** and **2** from PBE0 functional are more close to the experimental data.[19] At PBE0, the adsorption spectra at gas phase are less competitive (inferior) compared with those in solution (Table S4). In addition, based on the optimized geometries from PBE0, B3LYP and M052X, it is seen that PBE0 also gives better performance in reproducing the experimental data, although the data from the optimized geometries of the other two methods are also satisfactory (Table S5).

Table 3 lists the most leading singlet excited states (with larger CI coefficients) and the triplet state associated with their

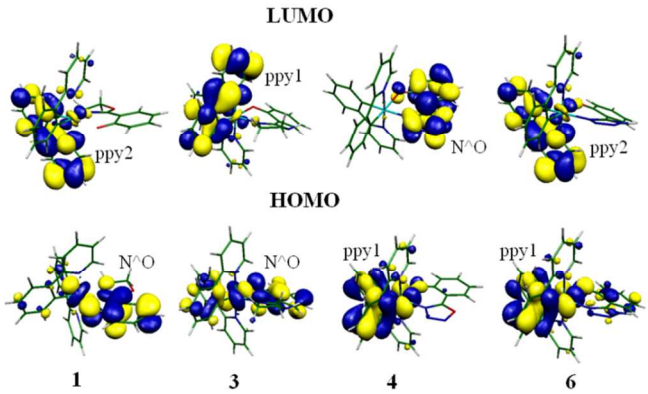

Fig. 3 HOMO and LUMO surfaces for complexes **1, 3, 4** and **6** obtained from DFT calculations at their S_0 optimized geometries.

oscillator strengths, dominant orbital excitations and their assignments, along with the corresponding experimental data from PBE0 method. It is seen that the calculated maximum absorption peaks of the complexes **1** and **2** at 250 and 248 nm are comparable to the experimental values[19] 249 and 243nm, respectively. This indicated that our calculated absorption spectra reproduce the experimental data very well. For complex **1**, the lowest singlet-singlet transition primarily comes from HOMO → LUMO and HOMO-1 → LUMO with the absorption band at 412 nm. The HOMO of complex **1** extends to Ir, ppy and oz ligands, whereas the LUMO is mainly localized on ppy ligands. Thus, the lowest-lying absorption can be described as metal to ligand charge transfer (MLCT)/intraligand charge transfer (ILCT)/ligand to ligand charge transfer (LLCT). The lowest-lying absorption band of **2** is similar to **1** with the character of MLCT/ILCT/LLCT. Compared with **1** and **2**, the lowest-lying absorption of **3** is slightly red-shifted. The results in Table 3 also show that the lowest-lying absorption of **4** is almost identical to that of the complex **1**. However, the lowest-lying absorption of **5** and **6** changed significantly compared with that of **2** and **3**. It was found that the wavelength of **5** is red-shifted by 65 nm compared with that of **2**. On the other hand, the wavelength of **6** is blue-shifted by 21 nm as compared to that of **3**. This suggests that the lowest-lying singlet-singlet absorptions are influenced by N^O ancillary ligands, which is consistent with the trend of the HOMO-LUMO energy gaps.

Meanwhile, the calculated absorption peaks with the largest oscillator strengths in **1** is localized at 250 nm. The transition configuration of HOMO-3 → LUMO+4 and HOMO → LUMO+5 contributes to the 250 nm absorption described as MLCT/ILCT/LLCT. Compared with **1**, the transitions with the largest oscillator strengths in **3** is slightly blue-shifted, while that of **4** is slightly red-shifted (Table 3). For **2**, **5** and **6**, the maximum absorption peaks are similar to that of **1**. In the transition $S_0 \rightarrow T_1$, the absorption band of **1** located at 467 nm is contributed by HOMO → LUMO and HOMO-1 → LUMO transitions with the character of MLCT/ILCT/LLCT. The calculated lowest triplet absorptions of **2** is at 498 nm, with the main transitions being found to be HOMO → LUMO+2 and HOMO-1 → LUMO+2. The calculated

Table 3 Calculated wavelength (nm), oscillator strength (*f*) and dominant orbital excitations of the lowest singlet and triplet vertical absorptions for the complexes **1-6**

	state	λ_{cal}	*f*	Configuration	Character	Exp.[19]
1	S_1	412	0.0370	H-1->LUMO (16%),	MLCT/ILCT/LLCT	
				HOMO->LUMO (77%)	MLCT/LLCT/ILCT	
	S_{33}	250	0.2973	H-3->L+4 (21%)	MLCT/ILCT/LLCT	249
				HOMO->L+5(34%)	MLCT/LLCT/ILCT	
	T_1	467	0.0000	H-1->LUMO (25%),	MLCT/ILCT/LLCT	
				HOMO->LUMO (36%)	MLCT/LLCT/ILCT	
2	S_1	412	0.0402	H-1->LUMO (12%),	MLCT/ILCT/LLCT	
				HOMO->LUMO (84%)	MLCT/LLCT/ILCT	
	S_{39}	248	0.1534	H-1->L+5 (15%),	MLCT/LLCT/ILCT	243
				HOMO->L+5 (11%),	MLCT/ILCT/LLCT	
				HOMO->L+6 (34%)	MLCT/LLCT/ILCT	
	T_1	498	0.0000	H-1->L+2 (18%),	MLCT/LLCT/ILCT	
				HOMO->L+2 (66%)	MLCT/ILCT/LLCT	
3	S_1	421	0.0344	HOMO->LUMO (85%)	MLCT/LLCT/ILCT	
	S_{40}	242	0.1956	H-5->L+3 (11%),	MLCT/LLCT/ILCT	
				HOMO->L+7 (37%)	MLCT/LLCT/ILCT	
	T_1	472	0.0000	H-1->LUMO (17%),	MLCT/LLCT/ILCT	
				HOMO->LUMO (46%)	MLCT/LLCT/ILCT	
4	S_1	413	0.0058	HOMO->LUMO (98%)	MLCT/LLCT/ILCT	
	S_{32}	256	0.2100	H-8->LUMO (13%),	ILCT	
				H-7->LUMO (48%)	ILCT/LLCT	
	T_1	521	0.0000	H-1->LUMO (88%)	MLCT /ILCT	
5	S_1	477	0.0118	HOMO->LUMO (99%)	MLCT/LLCT/ILCT	
	S_{38}	251	0.2055	H-2->L+4 (28%),	ILCT	
				HOMO->L+5 (31%)	MLCT/LLCT/ILCT	
	T_1	593	0.0000	H-1->LUMO (64%),	MLCT/ILCT/LLCT	
				HOMO->LUMO (29%)	MLCT/LLCT/ILCT	
6	S_1	400	0.0666	H-1->LUMO (11%),	MLCT/ILCT/LLCT	
				HOMO->LUMO (77%)	MLCT/LLCT/ILCT	
	S_{34}	251	0.2273	H-8->LUMO (26%),	LLCT	
				H-4->L+4 (34%)	MLCT/ILCT/LLCT	
	T_1	461	0.0000	H-2->L+1 (17%),	ILCT	
				H-1->LUMO (14%),	MLCT/LLCT/ILCT	
				HOMO->LUMO (27%),	MLCT/ILCT/LLCT	
				HOMO->L+1 (19%)	MLCT/ILCT/LLCT	

lowest triplet absorptions for **3**, **4**, **5** and **6** are at 472, 521, 593 and 461 nm, respectively. The configurations of **3** and **5** are the same with **1**, which occur from HOMO → LUMO and HOMO-1 → LUMO, with mixed nature of MLCT/ILCT/LLCT. Different from 1 and 2, the transition characters of 4 and 6 are MLCT/ILCT, MLCT/LLCT/ILCT, respectively. The non-negligible MLCT is beneficial for efficient intersystem crossing, and singlet-triplet transitions are expected to enhance the quantum efficiency for these Ir(III) complexes**.**

3.4 Phosphorescence properties

As mentioned in the computational methodology, TDDFT/M052X (in CH_2Cl_2 media) was selected to study the phosphorescent emissions of all the studied complexes since it could reproduce the experimental phosphorescent spectra reasonably. The calculated phosphorescent emissions for **1-6** are shown in Table 4, together with the electron transition assignments, and the experimental data.

The calculated lowest-energy emissions of the complexes **1** and **2** are localized at 498 and 595 nm. Upon the substitution of C atom with N atom on N^O ligands, the emission wavelength of **4** and **5** (546 and 619 nm) are red-shifted. However, the emission wavelengths of **3** (494 nm) in which N atom substitutes for O/S atom on N^O ligand and **6** (439 nm) are blue-shifted compared to complex **1**, in which

Table 4 Calculated phosphorescent emission wavelength (in nm) of the complexes **1-6** in CH_2Cl_2 media with the TDDFT method, along with the experimental data

	λ_{cal}	Configuration	Character	Exp.[19]
1	498	H-2->LUMO(28%),	MLCT/ILCT/LLCT	527
		H-1->LUMO(14%),	MLCT/ILCT/LLCT	
		HOMO->LUMO (43%)	MLCT/LLCT/ILCT	
2	595	H-1->LUMO(12%),	MLCT/ILCT/LLCT	542
		HOMO->LUMO (74%)	MLCT/LLCT/ILCT	
3	494	H-2->LUMO(27%),	MLCT/LLCT/ILCT	
		H-1->LUMO(14%),	MLCT/LLCT/ILCT	
		HOMO->LUMO (44%)	MLCT/LLCT/ILCT	
4	546	H-1->LUMO(15%),	MLCT/ILCT	
		HOMO->LUMO (77%)	MLCT/LLCT	
5	619	H-1->LUMO(33%),	MLCT/ ILCT	
		HOMO->LUMO (60%)	MLCT/LLCT	
6	439	H-1->LUMO(14%),	MLCT/LLCT/ILCT	
		H-1->L+1(31%),	MLCT/LLCT/ILCT	
		HOMO->LUMO(18%),	MLCT/ILCT/LLCT	
		HOMO->L+1 (15%)	MLCT/ILCT/LLCT	

the wavelength 439 nm lies in the deep blue region. This revealed that the N^O ligands in the studied complexes could modify the emission color from green and yellow to deep blue. The calculated lowest emission energy for **1** corresponds to the HOMO-2 → LUMO, HOMO-1 → LUMO and HOMO → LUMO transitions with mixed nature of MLCT/ILCT/LLCT. The configuration of **3** is the same as that of **1**. For **4** and **5**, there are two transitions contributing to calculated lowest emission, which are HOMO → LUMO and HOMO-1→LUMO transitions, respectively. The emission can be assigned as MLCT/ILCT/LLCT. For **6**, the emission is from HOMO-1 → LUMO+1, HOMO → LUMO, HOMO → LUMO+1 and HOMO-1 → LUMO, and is assigned as MLCT/LLCT/ILCT. The larger participation of Ir(III) center in the emissive state is expected to result in a high quantum efficiency.

3.5 Quantum efficiency

The emission quantum yield (Φ_{PL}) is linked to the radiative (k_r) and nonradiative (k_{nr}) rate constants, which can be expressed by equation (1), where τ_{em} is the emission decay time:

$$\Phi_{PL} = k_r \tau_{em} = \frac{k_r}{k_r + k_{nr}} \quad (1)$$

Accordingly, a large k_r and a small k_{nr} are required for a high quantum yield. Theoretically, k_r is related to the mixing between S_1 and T_1, which is proportional to the spin-orbit coupling (SOC) and inversely proportional to the energy difference between the two states expressed by equation (2):[37,38]

$$k_r = \gamma \frac{\langle \psi_{S1} | H_{SO} | \psi_{T1} \rangle^2 \times \mu_{S1}^2}{(\Delta E_{S1-T1})^2} \qquad \gamma = \frac{16\pi^3 10^6 n^3 E_{em}^3}{3h\varepsilon_0} \quad (2)$$

Here μ_{S1} is the transition electric dipole moment in $S_0 \rightarrow S_1$ transition, E_{em} represents the emission energy in cm^{-1}, while n, h and ε_0 are the refractive index, Planck's constant and the permittivity in vacuum, respectively. The heavy atom participation, such as iridium, is believed to increase the SOC effects and the intersystem crossing (ISC), provided that its orbitals make a significant contribution in the excited states involved.[39] Therefore, on one hand, the SOC effects can be elucidated by the contribution of MLCT in the T_1 state.[40] An increase of MLCT character can enhance SOC and hence the transition probability which would result in a drastic decrease of the radiative lifetime and avoid the nonradiative process.[41,42] Thus a large MLCT contribution will benefit for a high quantum yield (Φ_{PL}). The MLCT% values calculated as described in the work by Chou et al[43] are listed in Table 5. It can be found that the relative high Φ_{PL} values of **1** (0.55) compared with **2** (0.27) can be rationalized by the significant larger MLCT% of **1** (31.84%) than that of **2** (20.67%). In addition, from **3** to **6** with the incorporation of different N^O ligands, the MLCT% values increase, especially for **3** and **4**, indicating high Φ_{PL} can be achieved.

On the other hand, the SOC effects also can be elucidated by the singlet-triplet splitting energy (ΔE_{S1-T1}).[44–47] The $S_1 \rightarrow T_1$ intersystem crossing induced by SOC plays an important role in phosphorescent process. Equation (2) shows that the decreasing ΔE_{S1-T1} leads to higher radiative rates, while a decreasing μ_{S1} lowers k_r. Using equation (2), we recently provided a valuable theoretical analysis of the evolution of Φ_{PL} within a series of complexes[48] with the aid of computed ΔE_{S1-T1} and μ_{S1}. The calculated ΔE_{S1-T1} and μ_{S1} values are also shown in Table 5. The results indicated that the μ_{S1} value of **2** is slightly larger than that of **1**, which can not explain the high Φ_{PL} reported for **1**.[19] The much smaller ΔE_{S1-T1} value for **1** accounts for the higher Φ_{PL} compared with **2**. The ΔE_{S1-T1} for **3**, **5** and **6** were found to be relatively smaller than that of **2**, indicating that the N substitution in different N^O ligands is beneficial to enhance the ISC rate, and thus might increase Φ_{PL}. Of course, we should remember that besides the factors discussed above, other factors may also affect Φ_{PL} which are not taken into account in our discussion.

Table 5 The metal-based charge transfer character (MLCT, %), singlet-triplet splitting (ΔE_{S1-T1} in eV) and the transition dipole moment (μ_{S1} in a.u), along with experimental quantum yield Φ_{PL}

parameter	1	2	3	4	5	6
MLCT	31.84	20.67	32.62	34.90	31.32	23.77
μ_{S1}	0.5023	0.5455	0.4765	0.0791	0.1851	0.8776
ΔE_{S1-T1}	0.7497	0.9698	0.7084	1.0103	0.8919	0.7314
Φ_{PL}[19]	0.55	0.27				

4. Conclusion

DFT/TDDFT calculations have been performed to investigate the influence on electronic structure, absorption spectra, emission colour and quantum efficiency of the studied complexes induced by the introduction of different N^O ligands. In this study, the following conclusions can be drawn: (1) The composition of the LUMO is significantly affected, when the C-C bond is substituted with N-N bond. The existence of tetrazole ring of **6** leads to a large HOMO–LUMO energy gap. (2) Compared with **1** and **2**, the emission wavelengths for **4** and **5** are red-shifted, while they are blue-shifted significantly for **3** and **6**. Especially, the emission colour of the complex 6 is in deep blue region, which is promising as a blue-emmitting material. (3) The high quantum yield of **1** compared with **2** was found to be closely related to the large MLCT% and small ΔE_{S1-T1}. The results showed that the different ancillary ligands in **3**, **5** and **6** leads to a relatively large MLCT% and small ΔE_{S1-T1} and thus a high quantum yield. We hope that our results could provide constructive information for experimentalists in synthesizing high efficient phosphorescence materials.

Acknowledgements

The authors thank the financial support from the National Natural Science Foundation of China (Grant no. 21273219, 21221061, 21203174), Natural Science Foundation of Jilin Province (20140101045JC) and computing time from the High Performance Computing Center of Jilin University, China.

Notes and references

[a] *College of Resource and Environmental Science, Jilin Agricultural University, Changchun 130118, P. R. China.*
[b] *Institute of Condensed State Physics, Jilin Normal University, Siping 136000, P. R. China. E-mail: jhyang1@jlnu.edu.cn*
[c] *State Key Laboratory of Rare Earth Resource Utilization, Changchun Institute of Applied Chemistry, Chinese Academy of Sciences, Changchun 130022, P. R. China. E-mail: zjwu@ciac.ac.cn*
[d] *Université du Burundi, Faculté des Sciences, Département de Chimie, Bujumbura, BP.2700, Burundi.*

† Electronic Supplementary Information (ESI) available: Fig. S1: Contour plots of the HOMO and LUMO for complexes **2** and **5**. Table S1: Calculated phosphorescent emission wavelength (nm)/energies (eV) of the complexes **1** and **2** in CH_2Cl_2 media with the TDDFT method at the PBE0, M062X, M052X, B3LYP and Cam-B3LYP level, respectively, together with the experimental values. Table S2: Selected optimized parameters for complex **2** in the ground state from different density functionals. Table S3: Calculated absorption wavelength with the largest oscillator strengths for complexes **1** and **2** in CH_2Cl_2 media with the TDDFT method at the PBE0, B3LYP, M052X M062X and Cam-B3LYP level, respectively, together with the experimental data. Table S4: Calculated absorption wavelength (nm) and oscillator strength of the complexes **1** and **2** with the TDDFT method at the PBE0 level in gas phase and CH_2Cl_2 media, together with the experimental data. Table S5: Calculated absorption wavelength and oscillator strength of the complexes **1** and **2** with the TDDFT method at the PBE0 level using the PBE0, B3LYP and M052X optimized the ground state geometries, together with the experimental data. Tables S6-S11: Carrtesian coordinates for the optimized structures of **1-6** in the S_0 states. See DOI: 10.1039/b000000x/

1 S. Reineke, F. Lindner, G. Schwartz, N. Seidler, K. Walzer, B. Lussem and K. Leo, *Nature*, 2009, **459**, 234.
2 Y. C. Chiu, J. Y. Hung, Y. Chi, C. C. Chen, C. H. Chang, C. C. Wu, Y. M. Cheng, Y. C. Yu, G. H. Lee and P. T. Chou, *Adv. Mater.*, 2009, **21**, 2221.
3 M. Ikai, S. Tokito, Y. Sakamoto, T. Suzuki and Y. Taga, *Appl. Phys. Lett.*, 2001,**79**, 156.
4 C. Adachi, M. A. Baldo, M. E. Thompson and S. R. Forrest, *J. Appl. Phys.*, 2001, **90**, 5048.
5 Y. Chi and P. T. Chou,Chem. Soc. Rev., 2010,39, 638; P. T. Chou and Y. Chi, *Chem.–Eur. J.*, 2007, **13**, 380.
6 (a) Y. You, J. Seo, S. H. Kim, K. S. Kim, T. K. Ahn, D. Kim and S. Y. Park, *Inorg. Chem.*, 2008, **47**, 1476; (b) S. Tokito, T. Iijima, Y. Suzuri, H. Kita, T. Tsuzuki and F. Sato, *Appl. Phys. Lett.*, 2003, **83**,569; (c) W. Y. Wong and C. L. Ho, *Coord. Chem. Rev.*, 2009, **253**, 1709.
7 (a) W. Y. Wong, G. J. Zhou, X. M. Yu, H. S. Kwok and B. Z. Tang, *Adv. Funct. Mater.*, 2006, **16**, 838; (b) Z. Q. Chen, Z. Q. Bian and C. H. Huang, *Adv. Mater.*, 2010, **22**, 1534; (c) C. Ulbricht, B. Beyer, C. Friebe, A. Winter and U. S. Schubert, *Adv. Mater.*, 2009, **21**, 4418; (d) Y. You and S. Y. Park, *Dalton Trans.*, 2009, 1267; (e) X. Li, Q. Zhang, Y. Q. Tu, H. Agren and H. Tian, *Phys. Chem. Chem. Phys.*, 2010, **12**, 13730.
8 X. S. Zeng, M. Tavasli, I. F. Perepichka, A. S. Batsanov, M. R. Bryce, C. J. Chiang, C. Rothe and A. P. Monkman, *Chem.–Eur. J.*, 2008, **14**, 933.
9 L. He, L. Duan, J. Qiao, R. J. Wang, P. Wei, L. D. Wang and Y. Qiu, *Adv. Funct. Mater.*, 2008, **18**, 2123.
10 (a) Q. Zhao, S. J. Liu, M. Shi, C. M. Wang, M. X. Yu, L. Li, F. Y. Li, T. Yi and C. H. Huang, *Inorg. Chem.*, 2006, **45**, 6152; (b) S. J. Liu, Q. Zhao, R. F. Chen, Y. Deng, Q. L. Fan, F. Y. Li, L. H. Wang, C. H. Huang and W. Huang, *Chem.–Eur. J.*, 2006, **12**, 4351; (c) Q. Zhao, L. Li, F. Y. Li, M. X. Yu, Z. P. Liu, T. Yi and C. H. Huang, *Chem. Commun.*, 2008, 685; (d) S. J. Liu, Q. Zhao, B. X. Mi and W. Huang, *Adv. Polym. Sci.*, 2008, **212**, 125; (e) Q. Zhao, S. J. Liu and W. Huang, *Macromol. Rapid Commun.*, 2010, **31**, 794; (f) H. F. Shi, Y. Nakai, S. J. Liu, Q. Zhao, Z. F. An, T. Tsuboi and W. Huang, *J. Phys. Chem. C*, 2011, **115**, 11749.
11 M. A. Baldo, S. Lamansky, P. E. Burrows, M. E. Thompson and S. R. Forrest, *Appl. Phys. Lett.*, 1999, **75**,4.
12 R. J. Holmes, S. R. Forrest, Y. J. Tung, R. C. Kwong, J. J. Brown, S. Garon and M. E. Thompson, *Appl. Phys. Lett.*, 2003, **82**, 2422.
13 J. Li, P. I. Djurovich, B. D. Alleyne, M. Yousufuddin, N. N. Ho, J. C. Thomas, J. C. Peters, R. Bau and M. E. Thompson, *Inorg. Chem.*, 2005, **44**, 1713.
14 S. Okada, K. Okinaka, H. Iwawaki, M. Furugori, M. Hashimoto, T. Mukaide, J. Kamatani, S. Igawa, A. Tsuboyama, T. Takiguchi and K. Ueno, *Dalton Trans.*, 2005, 1583.
15 Y. Y. Lyu, Y. Byun, O. Kwon, E. Han, W. S. Jeon, R. R. Das and K. Char, *J. Phys. Chem. B*, 2006, **110**, 10303.
16 C. H. Yang, Y. M. Cheng, Y. Chi, C. J. Hsu, F. C. Fang, K. T. Wong, P. T. Chou, C. H. Chang, M. H. Tsai and C. C. Wu, *Angew. Chem., Int. Ed.*, 2007, **46**, 2418.
17 G. J. Zhou, W. Y. Wong, B. Yao, Z. Y. Xie and L. X. Wang, *Angew. Chem. Int. Ed.*, 2007, **46**, 1149.
18 C. L. Ho, W. Y. Wong, Q. Wang, D. G. Ma, L. X. Wang and Z. Y. Lin, *Adv. Funct. Mater.*, 2008, **18**, 928.
19 K.Chao, K.Z. Shao, T. Peng, D. X. Zhu, Y. Wang, Y. Liu, Z. M. Su, Martin R. Bryce, *J. Mater. Chem. C*, 2013, **1**, 6800.
20 C. F. Chang, Y. M. Cheng, Y. Chi, Y. C. Chiu, C. C. Lin, G. H. Lee, P. T. Chou, C. C. Chen, C. H. Chang and C. C. Wu, *Angew. Chem. Int. Ed.*, 2008, **47**, 4542.
21 S. J. Yeh, M. F. Wu, C. T. Chen, Y. H. Song, Y. Chi, M. H. Ho, S. F. Hsu and C. H. Chen, *Adv. Mater.*, 2005, **17**, 285.
22 E. Runge and E. K. U. Gross, *Phys. Rev. Lett.*, 1984, **52**, 997.
23 J. P. Perdew, K. Burke and M. Ernzerhof, *Phys. Rev. Lett.*, 1996, **77**, 3865.
24 J. P. Perdew, K. Burke and M. Ernzerhof, *Phys. Rev. Lett.*, 1997, **78**, 1396.
25 C. Adamo and V. Barone, *J. Chem. Phys.*, 1999, **110**, 6158.
26 (a) T. Liu, B. H. Xia, Q. C. Zheng, X. Zhou, Q. J. Pan and H. X. Zhang, *J. Comput. Chem.*, 2010, **31**, 628; (b) I. Ciofini, P. P. Laine, F. Bedioui and C. Adamo, *J. Am. Chem. Soc.*, 2004, **126**, 10763; (c)

I. Ciofini, P. P. Laine, F. Bedioui C. A. Daul and C. Adamo, C. R. Chim., 2006, **9**, 226; (d) D. Jacquemin, E. A. Perpete, G. Scalmani, M. J. Frisch, I. Ciofini and C. Adamo, *Chem. Phys. Lett.*, 2006, **421**, 272; (e) I. Ciofini, P. P. Laine, M. Zamboni, C. A. Daul, V. Marvaud and C. Adamo, *Chem. -Eur. J.*, 2007, **13**, 5360; (f) Y. L. Si, Y. Q. Liu, X. C. Qu, Y. Wang and Z. J. Wu, *Dalton Trans.*, 2013, **42**, 14149.

27 (a) J. Autschbach, T. Ziegler, S. J. A. Gisbergen and E. J. Baerends, *J. Chem. Phys.*, 2002, **116**, 6930; (b) T. Helgaker and P. Jørgemsen, *J. Chem. Phys.*, 1991, **95**, 2595; (c) K. L. Bak, P. Jørgemsen, T. Helgaker, K. Rund and H. J. A. Jensen, *J. Chem. Phys.*, 1993, **98**, 8873.

28 (a) E. Cancès, B. Mennucci and J. Tomasi, *J. Chem. Phys.*, 1997, **107**, 3032; (b) M. Cossi, V. Barone, B. Mennucci and J. Tomasi, *Chem. Phys. Lett.*, 1998, **286**, 253; (c) B. Mennucci and J. Tomasi, *J. Chem. Phys.*, 1997, **106**, 5151.

29 Y. Zhao and D.G. Truhlar, *J. Phys. Chem. A*, 2006, **110**, 5121.

30 Y. Zhao, N. E. Schultz, D. G. Truhlar, *J. Chem. Theory Comput.*, 2006, **2**, 364

31 A.D. Becke, *J. Chem. Phys.*, 1993, **98**, 5648; C.T. Lee, W. Yang, and R.G. Parr, *Phys. Rev.*, 1988, **B37**, 785.

32 T. Yanai, D. Tew and N. Handy, *Chem. Phys. Lett.*, 2004, **393**, 51.

33 P. C. Hariharan and J. A. Pople, *Mol. Phys.*, 1974, **27**, 209.

34 M. J. Frisch, G. W. Trucks, H. B. Schlegel, G. E. Scuseria, M. A. Robb, J. R. Cheeseman, G. Scalmani, V. Barone, B. Mennucci, G. A. Petersson, H. Nakatsuji, M. Caricato, X. Li, H. P. Hratchian, A. F. Izmaylov, J. Bloino, G. Zheng, J. L. Sonnenberg, M. Hada, M. Ehara, K. Toyota, R. Fukuda, J. Hasegawa, M. Ishida, T. Nakajima, Y. Honda, O. Kitao, H. Nakai, T. Vreven, J. A. Montgomery, Jr. J. E. Peralta, F. Ogliaro, M. Bearpark, J. J. Heyd, E. Brothers, K. N. Kudin, V. N. Staroverov, T. Keith, R. Kobayashi, J. Normand, K. Raghavachari, A. Rendell, J. C. Burant, S. S. Iyengar, J. Tomasi, M. Cossi, N. Rega, J. M. Millam, M. Klene, J. E. Knox, J. B. Cross, V. Bakken, C. Adamo, J. Jaramillo, R. Gomperts, R. E. Stratmann, O. Yazyev, A. J. Austin, R. Cammi, C. Pomelli, J. W. Ochterski, R. L. Martin, K. Morokuma, V. G. Zakrzewski, G. A. Voth, P. Salvador, J. J. Dannenberg, S. Dapprich, A. D. Daniels, O. Farkas, J. B. Foresman, J. V. Ortiz, J. Cioslowski and D. Fox, *J. Gaussian 09*, **Revision B.01**; Gaussian, Inc., Wallingford, CT, 2010.

35 U. Varetto, MOLEKEL Version, Swiss National Supercomputing Centre, Lugano Switzerland.

36 (a) H. R. Tsai, K. Y. Lu, S. H. Lai, C. H. Fan, C. H. Cheng, and I. C. Chen, J. *Phys. Chem. C*, 2011, **115**, 17163; (b) P. Jeffrey Hay, *J. Phys. Chem. A*, 2002, **106**, 1634; (c) A. R. G. Smith, M. J. Riley, S. C. Lo, P. L. Burn, I. R. Gentle, and B. J. Powell, *Phys. Rev. B*, 2011, **83**, 041105; (d) Y. L. Si, Y. Q. Liu, G. Gahungu, X. C. Qu and Z. J. Wu, *Mol. Phys.*, 2013, **111**, 3716.

37 S. Haneder, E. Da Como, J. Feldmann, J.M. Lupton, C. Lennartz, P. Erk, E. Fuchs, O. Molt, I. Munster, C. Schildknecht and G. Wagenblast, *Adv. Mater.*, 2008, **20**, 3325.

38 N. Turro, Modern Molecular Photochemistry, University Science Books, Palo Alto, CA, USA, 1991.

39 C.H. Yang, Y.M. Cheng, Y. Chi, C.J. Hsu, F.C. Fang, K.T. Wong, P.T. Chou, C.H. Chang, M.H. Tsai and C.C. Wu, *Angew. Chem. Int. Ed.*, 2007, **46**, 2418.

40 J. D. Chai and M. Head-Gordon, *Phys. Chem. Chem. Phys.*, 2008, **10**, 6615.

41 S. Sprouse, K. A. King, P. J. Spellane and R. J. Watts, *J. Am. Chem. Soc.*, 1984, **106**, 6647.

42 M. G. Colombo, T. C. Brunold, T. Riedener, H. U. Güdel, M. Förtsch and H. B. Bürgi, *Inorg. Chem.*, 1994, **33**, 545.

43 C. H. Lin, Y. Y. Chang, J. Y. Hung, C. Y. Lin, Y. Chi, M. W. Chung, C. L. Lin, P. T. Chou, G. H. Lee, C. H. Chang and W. C. Lin, *Angew. Chem. Int. Ed.*, 2011, **50**, 3182.

44 Z. F. Xie, F. Q. Bai, J. Wang and H. X. Zhang, *Mol. Phys.*, 2011, **109**, 1657.

45 P.J. Hay, *J. Phys. Chem. A*, 2002, **106**, 1634.

46 A. R. G. Smith, M. J. Riley, S. C. Lo, P. L. Burn, I. R. Gentle and B. J. Powell, *Phys. Rev. B: Condens. Matter*, 2011, **83 (1)**, 041105.

47 D. N. Kozhevnikov, V. N. Kozhevnikov, M. Z. Shafikov, A. M. Prokhorov, D. W. Bruce and J. A. G. Williams, *Inorg. Chem.*, 2011, **50**, 3804.

48 S. Zhang, Y. L. Si and Z. J. Wu, *RSC Adv.*, 2014, **4**,15849.

Modification of the emission colour and quantum efficiency for oxazoline- and thiazoline-containing Iridium complexes via different N^O ligands

Yanling Si[a], Shuai Zhang[a], Godefroid Gahungu[d], Jinghai Yang*[b] and Zhijian Wu*[c]

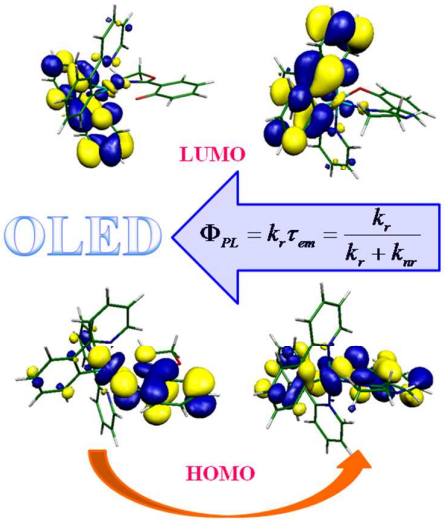

We present the electronic structure, absorption and emission spectra, as well as quantum efficiency of a series of oxazoline- and thiazoline-containing Ir(III) complexes to shed light on the effect of different N^O ligands on the emitting colour and quantum efficiency.